Korean J. Chem. Eng., 40(9), 2334-2341 (2023)
DOI: 10.1007/s11814-023-1452-9

pISSN: 0256-1115
eISSN: 1975-7220

Automated paint coating using two consecutive images with CNN regression

Byoung Chul Kim*, Jin Whan Park, and Young Han Kim**,†**

*Dept. of Chem. & Energy Eng., Kyungnam Coll. of Info. & Tech., Busan 47011, Korea
**Dept. of Industrial Chemistry, Pukyong National University, Busan 48547, Korea
(*Received 20 October 2022 • Revised 7 February 2023 • Accepted 14 March 2023*)

Abstract−Although new coating development for improved surface protection is necessary, its manual application has been a difficult problem to solve. In this study, a convolution neural network (CNN) was used for prediction of the painting gun operation. Painting videos were converted to sequential images, of which two consecutive images were associated with the gun position in the next time step. The inputs were implemented in a regression CNN training, which was used to calculate the position of the spray gun at the next moment. Recursive image utilization provides the prediction of spray gun movement in real-time applications. The statistical measures of the prediction and true values of gun movement using test data indicate that the proposed CNN gives comparable outcomes to similar applications of the CNN. The exhibition of simulated painting of a rectangle and a semicircle demonstrates the usefulness of the proposed CNN application for spray gun painting.

Keywords: Surface Coating, Paint Application, Convolution Neural Network, Motion Prediction

INTRODUCTION

The harsh occupational environment in industrial painting is harmful to human laborers [1,2]. As a result, predetermined painting processes handling fixed-sized applications, such as automotive and airplane parts, have been replaced with painting robots [3]. However, many places, including shipbuilding and large machinery assembly, require more flexible operation than can be provided by common machine painters because of the wide variation in the shape and size of painted objects. Autonomous robots are partially able to take over from human painters when human skills and experience are successfully transferred to the robots through deep learning technology [4]. Combining technologies of image collection and image processing with deep learning provides operational information for the robots in many applications. Crop detection [5] and waste classification [4] are good examples of industrial applications of connected technologies. This technology has also been utilized in medical diagnoses using images of patient diagnosis equipment [6-8].

One of the deep learning technologies, the convolution neural network (CNN), extracts features from images using a network trained with large sets of relevant images [9]. The image processing technique has been applied to chemical process development [10, 11]. The detected features have been analyzed for various applications, including facial recognition [12], crop detection [13,14], obstacle detection for unmanned aerial vehicles [15,16], forest classification for chemical leak tracking [17], finding an optimal condition in antioxidant fermentation [18], quantum computing in chemical engineering [19], nanofiltration design [20], metal-removal performance prediction [21], performance prediction in mass-transfer [22], and visual positioning [23,24]. While the existing applications of image processing with the CNN have used the computational results of the current state only, a predictive computation is available when the information of one step ahead is supplied to the CNN training. This one-step ahead prediction describes how spray gun is manipulated.

In this study, sequential images of gun movement in spray painting were used in the convolution neural network (CNN) prediction of the gun movement. One-step-ahead information of the 2D-location of the gun was utilized in the training of the vertically connected images of the present and one-step-before. The predictive computation of the gun position using the images and trained network was successively continued until the end of the painting operation. The performance was compared to the applications of regression CNN and demonstrated in simulated painting of a rectangle and a semicircle. The contributions of this study can be summarized as follows: (i) The regression CNN was implemented for motion prediction in paint coating; (ii) Connected sequential images were used for the motion prediction; (iii) Performance of the motion prediction was compared to other image regressions with the CNN.

METHODS

Automated manipulation of a spray gun requires its motion prediction, and the procedure is explained below.

1. Motion Prediction

Spray painting on a plain surface involves relatively simple movement of the spray gun holding paint. The coating has been developed for the improved protection of applied surface [25,26] and environmental atmosphere [27]. Mostly, the gun maintains a constant distance from the surface while spraying paint perpendicu-

Electronic supplementary material The online version of this article (https://doi.org/10.1007/s11814-023-1452-9) contains supplementary material, which is available to authorized users.

†To whom correspondence should be addressed.
E-mail: yhkim2@pknu.ac.kr

larly. It travels horizontally from one end of the surface to the other and moves vertically to begin the next line of spraying in the reverse direction of horizontal travel. The spraying pattern is maintained for a plain vertical surface, but the structural shape and dimensions of the painted surface are arbitrary. The movements of the spraying gun for various painting processes can be traced from sequential images sampled from a practical painting video at a constant sampling time. The spray technique was utilized in various thin film development [28,29].

A series of gun movements is described as

$$\Delta L_k = \tilde{L}_{k+1} - L_k \quad (1)$$

where L_k is the location of the gun at moment k, and the predicted location $\tilde{L}_{k+1}$ is obtained from the CNN prediction. The gun movements are sequentially connected for a painting job, in which the movement prediction at moment k is related to the precedent gun locations at the moments of k, k−1, and so on. A brief description of the CNN training and prediction of the gun location with time sequence is shown in Fig. 1. Because image inputs are implemented in the CNN for the prediction of gun location at moment k+1, a minimum number of images was used in this study. Two images at moments k−1 and k were vertically connected and used as the input to the CNN. Examples of the connected images are demonstrated in Fig. 2. Two 3-channel images are vertically arranged. The training of the CNN model utilized three consecutive images, of which the first two were applied to predict the motion of the spray gun. The prediction was validated with the motion calculated between the second and third images, which were provided in the training process for the deep learning model. In the calculation of

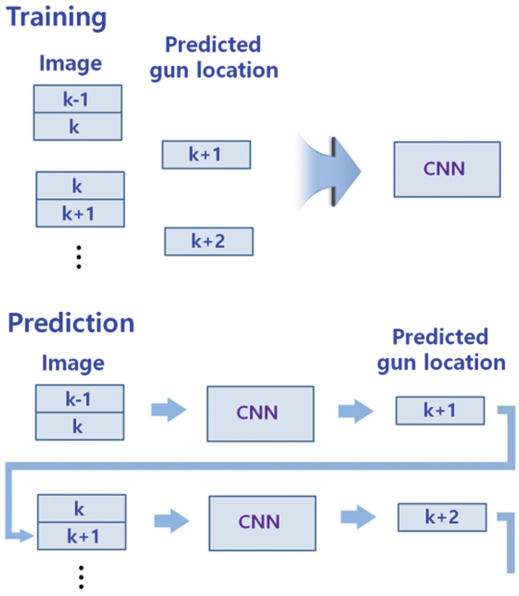

Fig. 1. Description of data flow in the CNN training and spray gun location prediction. Images are vertically connected, and k denotes temporal step in sequence.

gun movement used in the training, the tip of the paint gun was located with manually added green squares for accurate evaluation, as explained in the section on Data Sets and Preprocessing. When the trained model was ready, any two consecutive images predicted the gun motion at the next sequence, which was repeated until the intended painting was concluded. Although the images used in the

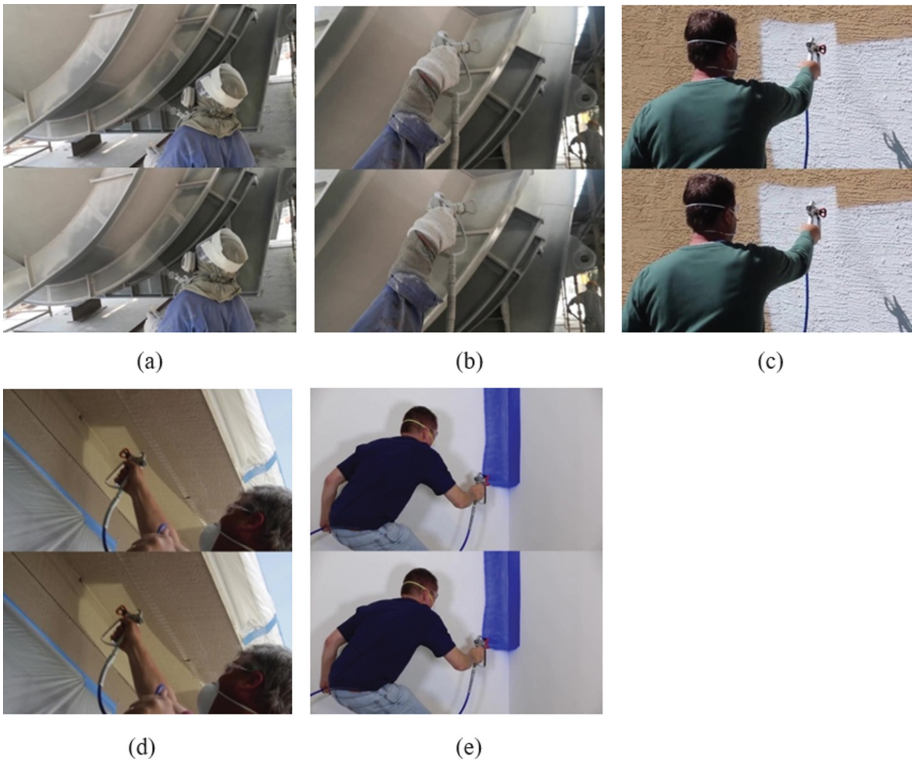

Fig. 2. Input images of spray gun painting, sets of two consecutive images; (a) and (b): industrial rotary kiln, (c), (d), and (e): wall painting.

training process differed from any prospective painting job, training with many practical paintings of different objects provided a useful process training for spray gun manipulation, as demonstrated in the three examples of demonstration provided in the Supporting Materials.

The images extracted from the original painting videos were processed by manual addition of very small green squares at the spray gun tip; the processing code and images are included in the Supporting Materials. The added green squares indicate the tip of the gun, where the paint is sprayed and applied to the object surface. Practical spray painting requires a perpendicular paint spray on the surface to ensure a clean painted surface and minimum loss of paint. Continuous painting is required for the best performance. The trajectories of the spray gun tip were scanned using green squares, and their speed was determined from the trajectories because the images were extracted at 24 frames per second. The time frame between the extracted images was constant at the video frame speed. As illustrated in Fig. 2, two videos were obtained from different painting jobs. A wide variety of videos are necessary for the model training. Although the painting images taken from the videos were sequential, the training process uses randomly shuffled training images for better performance, as in other studies [30].

2. Convolution Neural Network

The convolution operation is widely used in image processing, where the 2D matrix representing the image is convolved with a smaller 2D kernel matrix [13]. The CNN is composed of three layers: a filter bank layer, non-linearity layer, and feature pooling layer [31]. The filter bank layer includes many hidden layers, and each layer is connected to the adjacent layers. All the cells in a layer and those of one of the adjacent layers are linearly connected with the parameters. An RGB image input is a 3D array with 2D feature maps of the three channels. A trainable kernel (filter) k_{ij} in the filter bank connects the input feature map x_i to the output feature map y_i [31].

$$y_i = b_j + \Sigma_i k_{ij} * x_i \tag{2}$$

where $*$ is the 2D discrete convolution operator and b_j is a trainable bias parameter.

Non-linearity layers include a batch normalization layer [32] and a rectified linear unit layer [33]. The normalized activation is calculated as follows:

$$x_i = \frac{x_i - \mu_B}{\sqrt{\sigma_B^2 + \varepsilon}} \tag{3}$$

where μ_B is the mean, σ_B^2 is the variance, and ε is a stability constant. The normalized value is obtained from an offset and a scale factor and two learnable parameters, as follows:

$$y_i = \gamma \hat{x}_i + \beta \tag{4}$$

The feature pooling layers are dropout [34], fully connected [35], and regression layers [36]. The structure of the CNN with detailed information of filter size and number, stride and padding sizes, and output derivation is shown in Fig. 3.

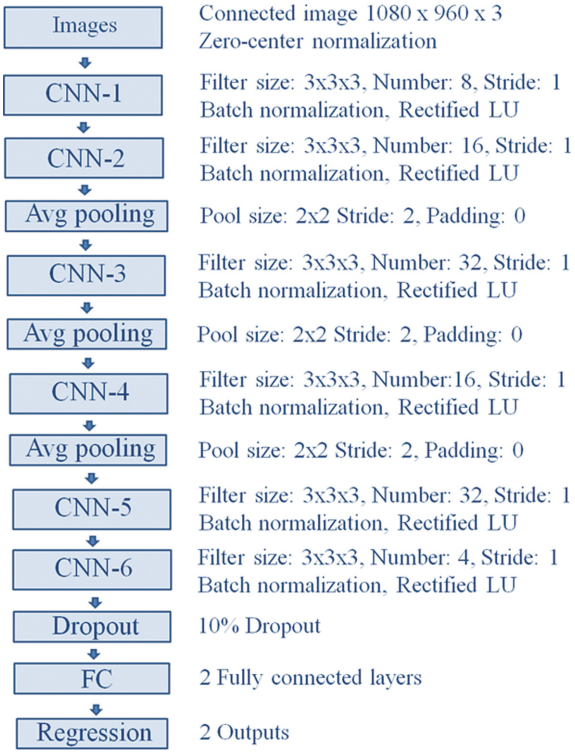

Fig. 3. Architecture of the proposed convolution neural network.

DEVELOPMENT

The detail of the motion prediction from a set of consecutive images using a trained CNN model was explained as follows.

1. Data Sets and Preprocessing

Two painting videos were used to extract still color images of size 960×540 pixels. Fig. 4 illustrates an example image with a small green square for gun position detection. The square was manually added, as explained below. Note that a set of two consecutive original images is connected, as shown in Fig. 2, and implemented in the CNN application. As explained in Fig. 1, gun location associated with each connected images was supplied to the CNN training, and the trained model was used to calculate a regression output. The manual positioning of green square was only applied for the model training. In the prediction of the gun movement, the manual procedure was not necessary.

For gun position detection, a small green square was manually

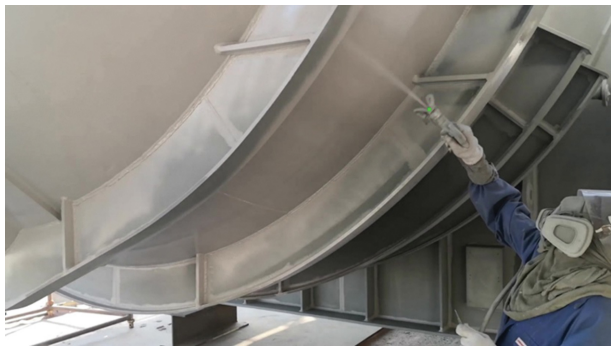

Fig. 4. Image of spray gun painting with a manually inserted green mark at the gun tip.

added to the gun tip. Locating solely the gun tip without the green mark was difficult using an image recognition tool, when it was searched in the original image. The RGB image was split to 3-color images, and the red image was subtracted from the green image to segregate the green mark only. The green image was used locating the mark. The movement of the spray gun was computed from the location of the gun tip. The location associated with the CNN input images (Fig. 2) was used to compute the predicted gun position using Eq. (1). The gun movement in the horizontal and vertical directions was the true value of the outputs in the CNN training. Data used in this project are provided in the Supporting Materials including videos used in training the CNN model, the images extracted from the videos, images with small green squares added images to detect the tip of the spray gun, python code to place the green squares, python code to locate the position of the tip of the spray gun, MATLAB code was used to train the CNN model, MATLAB data on the trained model, MATLAB code for the virtual painting, and three example painting videos.

The connected input images were randomized, and 20% were reserved as the test set, with the rest used in training. Note that the predicted gun movement calculated using Eq. (1) was associated with the images and was simultaneously randomized. The training data were randomized, and ten-fold cross validation was applied to improve network performance [30]. The randomized data were separated into ten groups: one sequentially selected group among the ten was used for validation, and the nine others were implemented in the training. After every 20 epochs of training and validation, the training data were randomized again, and the training and validation were continued until the root mean square error (RMSE) was stabilized.

2. Implementation Details

The input images were vertically connected 3-channel RGB images, and their sizes were determined considering the available size of the PC RAM memory. The network was trained and tested using MATLAB ver. 2019a. The training of the proposed CNN was conducted for 100 epochs with a randomized training dataset of training and validation sets in a ratio of 9 to 1, as suggested by the ten-fold cross validation [30] for improved performance. An input set of 2,458 and 273 images for training and validation, respectively, was used, and 682 images were separately implemented for testing. Randomized datasets were applied in alternate epochs. The detailed training parameters are listed in Table 1, and the CNN structure is shown in Fig. 3. The structure includes six CNNs, three average poolings, and 10% dropout to reduce overfitting. The spraying gun movement in the painting was classified in the horizontal and vertical directions, requiring two fully connected layers for the two output regressions.

Table 1. Parameters in training of the proposed convolution neural network

Name	Value
Learning rate drop factor	0.1
Learning drop period	20
Validation frequency	22
Shuffle	Every epoch
Learn rate schedule	Piecewise
Learn drop period	20
Initial learning rate	0.0001
Total epochs	100
Mini batch size	64
Solver	sgdm
Momentum	0.9

The network parameters were updated to minimize the loss function of the half-mean-squared-error of the predicted responses using a standard gradient descent algorithm with a momentum of 0.9. The optimization led to the direction of the negative gradient of the loss at a given learning rate. After the training was completed, the reserved test set of data was supplied to predict two output values for the horizontal and vertical motion of the spray gun using the trained network. When a painting job is assigned, the painting boundary is predetermined, and the painter follows the boundary limit. The initial position of the spray gun is established for the beginning of the procedure, usually at the top-left corner, and the first motion is a small horizontal movement in the right-hand direction. The first two images provide the first input image to the trained CNN model, which predicts horizontal and vertical movements. These two movements are performed until the horizontal position reaches the predetermined boundary, where the horizontal movement continues in the reverse direction with the predicted horizontal and vertical movements. A boundary restriction is applied to satisfy the target shape of the painting project. The painting process simulates the realistic operation of a spray gun by a human worker, as shown in the demonstration videos used to train the model. The simulation terminates when the vertical position reaches the bottom boundary of the assigned project. This restriction is applied at the boundaries of the target painting shape.

RESULTS AND DISCUSSION

The proposed procedure of the motion prediction of a spray painting gun was practically demonstrated, and its performance was compared to other image processing techniques utilizing the CNN in various fields of studies.

1. Performance Evaluation

Five example input images are shown in Fig. 2; the first two are of surface painting on an industrial rotary kiln, and the others are a demonstration of wall painting. The prediction performance of the proposed CNN was verified by applying a test set of data to the trained network. Fig. 5 shows the comparison between the actual movement and predicted movements in the horizontal and vertical directions. The actual movement was derived from the gun location detection a step forward to the connected inputs. The sequences are explained in Fig. 1. The movement was measured in pixel units, and the input images were 960×1080 pixels. The correlation coefficients between the actual and predicted values, shown in Fig. 5, were 0.935 and 0.961 for the horizontal and vertical directions, respectively. Because the actual movement in practical spray painting was greater than 10 pixels in 960×1080 pixel images in many cases, the limited cases in Fig. 5 were larger in actual movements. Increasing the limit improves the prediction accuracy at the limits,

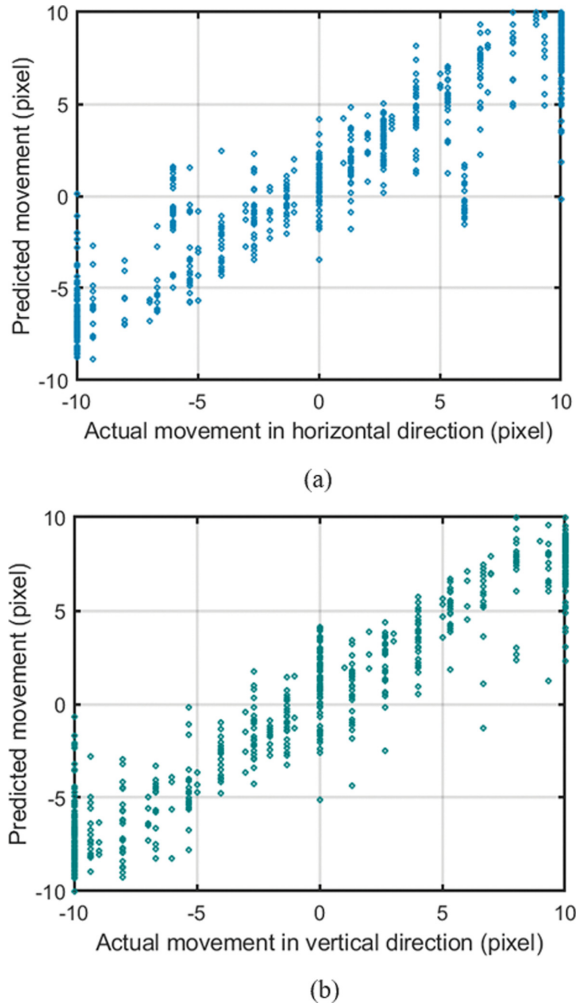

Fig. 5. Comparison of actual and predicted movements in horizontal and vertical directions, (a) horizontal, (b) vertical.

but a large predicted movement may induce erroneous painting in practical implementations. Therefore, this limit was set in the present study. The actual movement was counted using discrete pixel numbers. Although the accuracy could be increased by applying a continuous actual value in the training process and in movement prediction, the image processing used in this study was limited to pixel-based analysis. Therefore, discrete counts of movement were used in the training process and in motion prediction. Because the output prediction using a regression CNN for the connected image input has not yet been reported, the outcome of this study was not directly evaluated with published reports in comparison.

Although feature detection and classification from images have been reported in many studies [37,38], the application of regression CNN to the images is uncommon due to difficult quantification of the feature. The performance of this study was also evaluated with results of regression CNN in other applications. In the prediction of athlete ground reaction forces and moments, locations of eight labeled markers were supplied to spatio-temporal driven CNNs. The actual ground reaction forces and moments were computed from high-speed video camera vision of sensors attached on an athlete. The measured and predicted values with a trained CNN regression model were compared with the results of correlation coefficients between 0.973 and 0.988 for mean forces and between 0.941 and 0.972 for mean moments [39]. While eight markers were used in the simulated images of the study, the current study accommodated one non-distinctive marker, the spray gun, which explained the lower coefficients in this study.

In another study, a sequential organ failure assessment was conducted using seven vital signs for 12 time intervals as the input set of data to the regression CNN [40]. The predicted failure assessment with a trained CNN model data imputation using the principal component analysis (PCA) method was compared to the actual failure assessment from real diagnostic evaluation with the full vital signals, and the correlation coefficient was 0.863, which was lower than that in this study. A summary of the CNN outlines and performance indices in comparison with the regression CNN studies is listed in Table 2.

The coefficients of determination between the actual and predicted values of this study were 0.835 and 0.895 for the horizontal and vertical directions, respectively. Measurements using electronic equipment and color features were converted to single channel input to the regression CNN, and the total soluble solid content and water content in oranges were estimated with help of a CNN model composed of measured results of spectrometer, machine vision, and e-nose [41]. The predicted values were compared to actual measurements of the contents, resulting in coefficients of determination of 0.858 and 0.703 for the total soluble solid content and water content, respectively. Although there are differences in input type, size, and training number for different applications, the

Table 2. Performance comparison in various applications of regression CNNs

Input type	Image size	Training number	Output	Corr. coef.	Coef. det.	Ref.
Simulated image	227×227×3	2,400	1	0.988		[39]
Numeric data	12×7	5,154	1	0.863		[40]
Numeric data	40×40	106	1		0.858	[41]
Numeric data	35×35	106	1		0.703	[41]
Image	512×512	250	1	0.84		[42]
Image	180×90	4,380	1	0.86		[43]
Image	2,220×2,220	2,856	1	0.822		[44]
Image	960×1,080×3	2,731	2	0.935	0.835	This study
				0.961	0.895	

compared indices indicate that the performance of the proposed CNN in the current study is comparable to that of previous studies. Note that numeric data were input to the CNN in the study and this study used image input.

As an image-used CNN application, a biomarker, chest computed tomography (CT) score, for COVID-19 pneumonia diagnosis was computed from the chest CT scan images and a CNN trained model, and the predicted scores were compared to the scores determined by experienced radiologists [42]. Those compared results showed a correlation coefficient of 0.84. In other image-processed CNN applications, the daily precipitation observed with rain gauges was compared to the estimates from four satellite precipitation products (SPPs) using a combined model of the geographically weighted regression and long short-term memory network, similar to the CNN [43], and the prediction had a correlation coefficient of 0.86. A mine rehabilitation was assessed with airborne 2D LiDAR images [44]. The prediction of rehabilitation surface status using the continuous surface data was derived from the classification of 2D LiDAR plots, and trained with the support vector machine algorithm and CNN. The comparison of the prediction with ground-truth plot data resulted in a goodness having a correlation coefficient of 0.822. As summarized in Table 2, the performance index comparison between the predicted and actual values indicates that the proposed procedure of this study showed mostly better performance than various other applications of the CNN in image and image-like data processing.

2. Discussion

For further performance examination, a simulated painting was conducted using the trained CNN in this study. Because spray gun movement was directly related to the painted outcome, the drawing of the gun movement was depicted as a picture. Two drawings, a rectangle and a semicircle, were sequentially drafted using the regression output of the CNN. The bounds of the pictures were supplied to the drawing program. The initial two pictures were manually assigned to the program to generate the first input image, a set of two consecutive images, which was supplied to the CNN to predict the gun movements in the horizontal and vertical directions. Using the prediction, the next image was drawn up, and the last single image of the current connected image and the newly drawn image were combined for the computation of the next gun movement. The prediction sequences are shown in Fig. 1. The computed gun position was supplied for a continuous picture drawing. Examples of the two test drawings of a rectangle and a semicircle are displayed in Fig. 6. Each of them has two consecutive images in the painting process showing the horizontal progress of painting. A motion prediction for painting a triangle is presented in Fig. 6(c), and the video images of the three example paintings and other necessary materials are provided in the Supporting Materials. The consecutive painting of the three designated shapes demonstrates how the proposed procedure was applied in practical spray painting. The video demonstrates the practical application of the proposed CNN model and the associated procedure for clarity. The resulting motion of the spray gun is demonstrated in the videos provided in the Supporting Materials. Although the painted boundaries were irregular and unfinished areas were found in the final image, the gun motion in the horizontal and vertical directions showed how

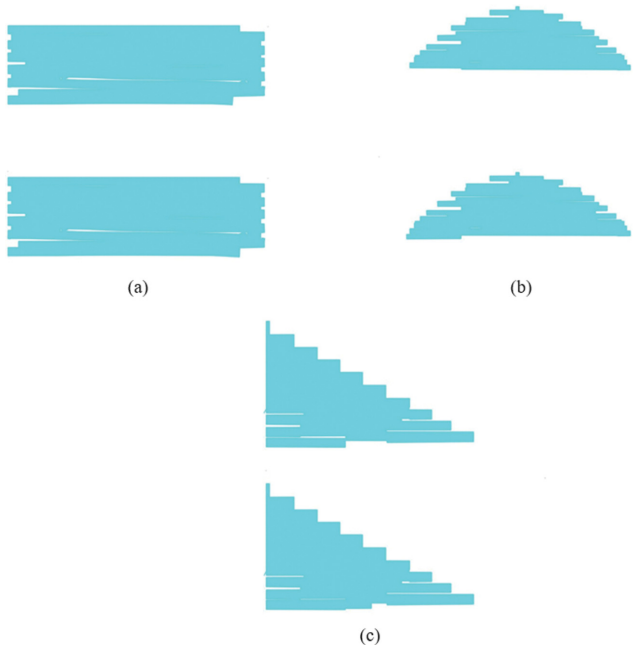

Fig. 6. Simulated painting using the pattern of motion predicted by the proposed CNN. Two consecutive images indicate the horizontal movement of the spray gun. The subfigures show (a) rectangle, (b) semicircle, and (c) triangle shapes.

the CNN model managed the gun movement for the given shape. The process of the three example shape drawings was not used in the training of the CNN. When a similar process of simple shape drawings is additionally applied to the training, the performance of the drawing can be improved.

In recent studies on image processing, convolution neural networks (CNN) are among the most widely used models [45-50]. Although we compared the performance of image processing methods provided in other studies using CNNs (Table 2), these applications differed considerably in terms of the preparation of input images and the dimensionality of the regression results. As listed in Table 2, two-dimensional regression was the only result among the studies. While other studies analyzed individual images, the regression approach considered in this work utilized two consecutive images to predict one step ahead. Therefore, the CNN model provided two consecutive images results in advance, which were not presented previously. To evaluate the performance of the proposed approach, the training procedures of the CNN model were applied in different training, and the results for motion prediction are shown for comparison in Table 3. This comparison led to the working CNN model used in example paintings shown the best.

The gun movement prediction in this study was based on human experience connected with the CNN. For non-flat target surface applications, the distance between the gun tip and the target should be maintained constant, as suggested by practical painting skills. In the prediction of gun movement, two consecutive images of the current and previous moments were used, but using three or more consecutive images may provide a more accurate prediction. This would require more training time and a larger computing facility equipped with more RAM capacity and faster GPU devices. How-

Table 3. Comparison of prediction accuracy with different training cycles

Training cycles	Correlation coefficient	
	Horizontal motion	Vertical motion
15	0.926	0.961
22	0.905	0.960
36	0.934	0.957
37	0.935	0.961

ever, the use of the trained network computing gun movement in applications is not affected by the extended input application because of the same size of the trained network.

Many medical applications of CNN [6,7,42,51-54] have utilized image inputs of X-ray, CT scanning, and MRI inspections, but those studies limited their results to diagnostic purposes. The prediction with connected consecutive images of this study can be extended to medical applications for the purpose of prognosis. The limitation of available images and differences in the treatment of patients may cause a problem in the direct application of the prediction. Anonymizing medical records for large training data and modifying the CNN training by adding treatment modification as training input may solve the problems in the prediction. Although a self-driving system requires various information of road condition, lane following, speed and location of adjacent vehicles, expected turn requirement, speed limits, sudden change of situation, and avoiding accident, the proposed technique of motion prediction using consecutive, most recent images can provide a resilient driving prediction in automobile application. Most prior works on applications of CNN regression focused on processing single images or combinations of single images, in contrast to the present work, which focuses on using two sequential images. Moreover, previous works did not consider the prediction of the movement of the spray gun at the next step using deep learning. Using three consecutive images, the first two were combined as an input image for the CNN model, and the latter two images provided two regression outputs for the training process, including horizontal and vertical movements. With sufficient training of randomized image data, the trained CNN was able to predict the movement of the gun when two consecutive images with the same frame speed were used as input. Because motion prediction from images has not been studied in previous works, no prior methods were available with which to compare the performance of the proposed approach. An analysis of automobile driving can be conducted as a prospective application of this study; however, the scope of this application exceeds that of the present work. Given the comparison of the performance with other CNN applications of image processing in Table 2, the complexity and development impact of the proposed approach may be considered more advanced than those of existing methods.

Most CNN applications in image processing apply a single-image input for network training, but the motion prediction in this study, which is dynamic motion prediction, was difficult using single images because of the less accurate prediction of the gun motion. When two consecutive images of gun movement were applied in the network training, the prediction was more accurate than that of the single image application. Comparing two consecutive images provides precise movement data, which leads to better prediction in the next sequence. However, processing a single image does not yield any current movement information, and its next-moment prediction is even more difficult. To examine the narrative, the model training results of a single image and two consecutive image processing were investigated with their prediction performance using the proposed CNN network of this study. Table 4 compares the performances using different images. and single image processing yields non-comparable outcomes, as indicated by the limitations above. The correlation coefficients and coefficients of determination were computed from the gun movement in the training images used in the CNN model. The values of CNN prediction and actual movement in the horizontal and vertical directions were correlated for single- and two-image inputs to the CNN training and prediction. The application of the two consecutive images clearly demonstrated its effectiveness. The proposed two-image CNN model application was useful for the dynamic prediction of any moving process, such as spray-gun painting.

Table 4. Regression performance with single and consecutive two-image inputs for CNN network training

Input type	Corr. coef.		Coef. det.	
	Horizontal	Vertical	Horizontal	Vertical
Single image	0.426	0.614	0.083	0.353
Two images	0.935	0.961	0.835	0.895

As augmented reality provides the chemical process engineers with an overview of the ageing state of the critical equipment during their inspection [55], the proposed image-processing procedure can provide predictive information of possible equipment ageing and fault detection. A collected image database of chemical plant fault detection and equipment failure is a useful source of an application of the proposed image-processing technique.

CONCLUSION

Two consecutive painting images were used to predict the manipulation of a spray gun using a regression CNN. Two sequential images of practical painting were iteratively connected and supplied to the CNN for training. The gun location in the training images was obtained from a manually labelled gun tip. Using two sequential images, the next gun movement was predicted using the trained CNN. The performance of gun movement prediction was compared to similar regression CNN applications, leading to comparable results in terms of the correlation coefficient and coefficient of determination between the measured and predicted values. Two simulated painting video demonstrations using bounded rectangles and semicircles showed that the gun operation predicted with the proposed regression CNN is viable for implementation in autonomous robot painters. Overall, it was proved that the connected image inputs effectively provided a one-step next movement without additional data processing using a regression CNN that could be utilized in other applications, such as chemical process hazard diagnosis, automobile self-driving, and medical prognosis.

ACKNOWLEDGEMENTS

Support from the Basic Science Research Program through the Korea Coating Technology Center is gratefully acknowledged.

REFERENCES

1. Y. Chen, W. Z. Chen, B. Li, G. Zhang and W. M. Zhang, *Ind. Robot.*, **44**, 629 (2017).
2. V. Prabakaran, A. V. Le, P. T. Kyaw, R. E. Mohan, P. Kandasamy, T. N. Nguyen and M. Kannan, *IEEE Access*, **8**, 193790 (2020).
3. Y. A. Wang, X. P. Xie and X. H. Lu, *Coatings*, **10**, 475 (2020).
4. D. O. Melinte, A. M. Travediu and D. N. Dumitriu, *Appl. Sci.-Basel*, **10**, 7301 (2020).
5. J. Champ, A. Mora-Fallas, H. Goeau, E. Mata-Montero, P. Bonnet and A. Joly, *Appl. Plant Sci.*, **8**, 1 (2020).
6. Q. Zhang, E. Hann, K. Werys, C. Wu, I. Popescu, E. Lukaschuk, A. Barutcu, V. M. Ferreira and S. K. Piechnik, *Artif. Intell. Med.*, **110**, 101955 (2020).
7. S. P. Singh, L. P. Wang, S. Gupta, H. Goli, P. Padmanabhan and B. Gulyas, *Sensors*, **20**, 5097 (2020).
8. M. K. Abd-Ellah, A. I. Awad, A. A. M. Khalaf and H. F. A. Hamed, *Eurasip J. Image and Video Process.*, **2018**, 1 (2018).
9. C. B. Murthy, M. F. Hashmi, N. D. Bokde and Z. W. Geem, *Appl. Sci.-Basel*, **10**, 3280 (2020).
10. A. Seshadri, S. Mahadevan and V. Muniyandi, *Korean J. Chem. Eng.*, **32**, 826 (2015).
11. N. Dehghan, M. A. Tavanaie and P. Payvandy, *Korean J. Chem. Eng.*, **32**, 1928 (2015).
12. C. Kendrick, K. Tan, K. Walker and M. H. Yap, *Symmetry-Basel*, **10**, 230 (2018).
13. J. Naranjo-Torres, M. Mora, R. Hernandez-Garcia, R. J. Barrientos, C. Fredes and A. Valenzuela, *Appl. Sci.-Basel*, **10**, 3443 (2020).
14. Z. Z. Zhang, E. Kayacan, B. Thompson and G. Chowdhary, *Auton. Robot.*, **44**, 1289 (2020).
15. S. Back, G. Cho, J. Oh, X. T. Tran and H. Oh, *J. Intell. Robot. Syst.*, **100**, 1195 (2020).
16. H. Y. Lee, H. W. Ho and Y. Zhou, *J. Intell. Robot. Syst.*, **101**, 5 (2021).
17. H. Kim, A. L. Gebreselassie, S. Dan and D. Shin, *Korean J. Chem. Eng.*, **35**, 1231 (2018).
18. C. Joshi and R. S. Singhal, *Korean J. Chem. Eng.*, **35**, 195 (2018).
19. A. Ajagekar and F. Q. You, *Korean J. Chem. Eng.*, **39**, 811 (2022).
20. M. R. S. Emami, M. K. Amiri and S. P. G. Zaferani, *Korean J. Chem. Eng.*, **38**, 316 (2021).
21. A. Daghbandan, B. A. Souraki and M. A. Zadeh, *Korean J. Chem. Eng.*, **39**, 628 (2022).
22. F. Hosseini and M. Rahimi, *Korean J. Chem. Eng.*, **37**, 411 (2020).
23. Q. Liu and F. H. Duan, *J. Intell. Robot. Syst.*, **99**, 115 (2020).
24. Q. Zhou and X. Li, *J. Intell. Robot. Syst.*, **98**, 603 (2020).
25. T. H. Nguyen, N. T. Mai, V. R. M. Reddy, J. H. Jung and N. T. N. Truong, *Korean J. Chem. Eng.*, **37**, 1803 (2020).
26. A. Krishnan, *Korean J. Chem. Eng.*, **39**, 2861 (2022).
27. A. Noreen, K. M. Zia, M. Zuber, S. Tabasum and M. J. Saif, *Korean J. Chem. Eng.*, **33**, 388 (2016).
28. B. J. Jeon, S. W. Kang and J. K. Lee, *Korean J. Chem. Eng.*, **23**, 854 (2006).
29. H. Lee, D. S. Jeong, T. Mun, B. Pejjai, V. M. Reddy, T. J. Anderson and C. Park, *Korean J. Chem. Eng.*, **33**, 2486 (2016).
30. M. Kuhn and K. Johnson, *Applied predictive modeling*, Springer, New York (2013).
31. Y. LeCun, K. Kavukcuoglu and C. Farabet, *Proceedings of 2010 IEEE Intern. Symp. Circ. Syst.*, 11463159 (2010).
32. S. Ioffe and C. Szegedy, *arXiv*, 150203167 (2015).
33. B. Liu, Y. Zhang, D. J. He and Y. X. Li, *Symmetry-Basel*, **10**, 11 (2018).
34. N. Srivastava, G. Hinton, A. Krizhevsky, I. Sutskever and R. Salakhutdinov, *J. Mach. Learn. Res.*, **15**, 1929 (2014).
35. X. Glorot and Y. Bengio, *Proceedings of the thirteenth intern. Conf. artif. Intell. Stat.*, 249 (2010).
36. C. Szegedy, A. Toshev and D. Erhan, *Adv. Neural Inf. Process. Sys.*, Curran Associates Inc., San Francisco, 2553 (2013).
37. F. Jia, X. C. Tai and J. Liu, *Inverse Probl. Imaging*, **14**, 891 (2020).
38. D. Wen, P. Li, Y. H. Zhou, Y. B. Sun, J. Xu, Y. J. Liu, X. L. Li, J. H. Li, Z. J. Bian and L. Wang, *IEEE Trans. Neural Syst. Rehabil. Eng.*, **28**, 1702 (2020).
39. W. R. Johnson, J. Alderson, D. Lloyd and A. Mian, *IEEE Trans. Biomed. Eng.*, **66**, 689 (2019).
40. T. Asuroglu and H. Ogul, *Comput. Meth. Programs Biomed.*, **198**, 105816 (2021).
41. S. Xu, H. Z. Lu, C. Ference and Q. Q. Zhang, *Electronics*, **10**, 80 (2021).
42. P. Fervers, F. Fervers, A. Jaiswal, M. Rinneburger, M. Weisthoff, P. Pollmann-Schweckhorst, J. Kottlors, H. Carolus, S. Lennartz, D. Maintz, R. Shahzad and T. Persigehl, *Quant. Imaging Med. Surg.*, **12**, 5156 (2022).
43. J. M. Shen, P. Liu, J. Xia, Y. J. Zhao and Y. Dong, *Remote Sens.*, **14**, 3939 (2022).
44. X. Murray, A. Apan, R. Deo and T. Maraseni, *Geocarto Int.*, 1 (2022).
45. D. S. Joseph, P. M. Pawar and R. Pramanik, *Multimed. Tools Appl.* (2022), doi:10.1007/s11042-022-14004-6.
46. A. Namoun, A. Tufail, M. Y. Khan, A. Alrehaili, T. A. Syed and O. BenRhouma, *Sustainability*, **14**, 13578 (2022).
47. M. Sasaki, J. Muguro, F. Kitano, W. Njeri and K. Matsushita, *Appl. Sci.-Basel*, **12**, 10277 (2022).
48. F. Fardian, M. Mawarpury, K. Munadi and F. Arnia, *IEEE Access*, **10**, 96476 (2022).
49. S. Maurya, S. Tiwari, M. C. Mothukuri, C. M. Tangeda, R. N. S. Nandigam and D. C. Addagiri, *Biomed. Signal Process. Control*, **80**, 104398 (2023).
50. H. Z. Jin, C. Yu, Z. B. Gong, R. J. Zheng, Y. A. Zhao and Q. W. Fu, *Biomed. Signal Process. Control*, **79**, 104104 (2023).
51. X. H. Ren, T. T. Li, X. J. Yang, S. Wang, S. Ahmad, L. Xiang, S. R. Stone, L. H. Li, Y. Q. Zhan, D. G. Shen and Q. Wang, *IEEE J. Biomed. Health Inform.*, **23**, 2030 (2019).
52. D. Karimi, G. Nir, L. Fazli, P. C. Black, L. Goldenberg and S. E. Salcudean, *IEEE J. Biomed. Health Inform.*, **24**, 1413 (2020).
53. T. Kretz, K. R. Muller, T. Schaeffter and C. Elster, *IEEE Trans. Biomed. Eng.*, **67**, 3317 (2020).
54. K. Zhang, N. Liu, X. F. Yuan, X. Y. Guo, C. Gao, Z. B. Zhao and Z. Y. Ma, *IEEE Trans. Circuits Syst. Video Technol.*, **30**, 3140 (2020).
55. G. Ancione, R. Saitta, P. Bragatto, G. Fiumara and M. F. Milazzo, *Sustainability*, **14**, 6156 (2022).